HHS Public Access

Author manuscript

J Am Chem Soc. Author manuscript; available in PMC 2018 October 18.

Published in final edited form as:

J Am Chem Soc. 2017 October 18; 139(41): 14436–14442. doi:10.1021/jacs.7b06381.

Epigenetic DNA Modification N^6-Methyladenine Causes Site-Specific RNA Polymerase II Transcriptional Pausing

Wei Wang[†,#], **Liang Xu**[†,⊥,#], **Lulu Hu**[§], **Jenny Chong**[†], **Chuan He**[§], and **Dong Wang**[†,‡,*]

[†]Division of Pharmaceutical Sciences, Skaggs School of Pharmacy & Pharmaceutical Sciences, University of California, San Diego, La Jolla, California 92093-0625, United States

[‡]Department of Cellular & Molecular Medicine, School of Medicine, University of California, San Diego, La Jolla, California 92093-0625, United States

[§]Department of Chemistry and Institute for Biophysical Dynamics, Howard Hughes Medical Institute, The University of Chicago, Chicago, Illinois 60637, United States

[⊥]Department of Chemistry, Sun Yat-Sen University, Guangzhou 510275, China

Abstract

N^6-Methyladenine (N^6-mA or 6 mA) is an epigenetic DNA modification in eukaryotic genomes. In contrast to the well-established roles of 5-methylcytosine for epigenetic regulation of gene expression, the functional roles of N^6-mA remain elusive. In particular, the impact of N^6-mA modification of the DNA template on RNA polymerase II (pol II) transcription elongation is not known. In this work, using the *Saccharomyces cerevisiae* pol II transcriptional elongation system as a model, we investigated the molecular mechanism of pol II recognition and processing of N^6-mA sites via both biochemical and structural approaches. We found that N^6-mA causes site-specific pol II pausing/stalling. Structural analysis revealed that while N^6-mA can reach the +1 template position, the stability of the N^6-mA and UTP base pairing is compromised. Taken together, we reveal that the presence of the 6-methyl group on adenine reduces incorporation efficiency and promotes backtracking translocation. Our studies with yeast pol II provide molecular insights into understanding the impacts of N^6-mA on pol II transcription dynamics in different organisms.

[*]Corresponding Author: dongwang@ucsd.edu.

[#]**Author Contributions**

Wei Wang and Liang Xu contributed equally.

ORCID

Dong Wang: 0000-0002-2829-1546

Accession Codes

The atomic coordinates and structure factors have been deposited in Protein Data Bank with accession codes of 5W4U (EC-I) and 5W51 (EC-II).

Notes

The authors declare no competing financial interest.

Supporting Information

The Supporting Information is available free of charge on the ACS Publications website at DOI: 10.1021/jacs.7b06381.

Additional data of pol II pausing, quantitative analysis of observed kinetic rates for single UMP incorporation, data verifying UMP incorporation opposite N^6-mA site, analysis of TFIIS-stimulated transcript cleavage rates and patterns, crystal structure of EC-I complex, electron density maps of pol II EC-II and two conformations of UMPNPP, deconvoluted ESI mass spectrum characterization of synthetic N^6-mA containing DNA oligo, and X-ray diffraction data and refinement statistics (PDF)

Graphical Abstract

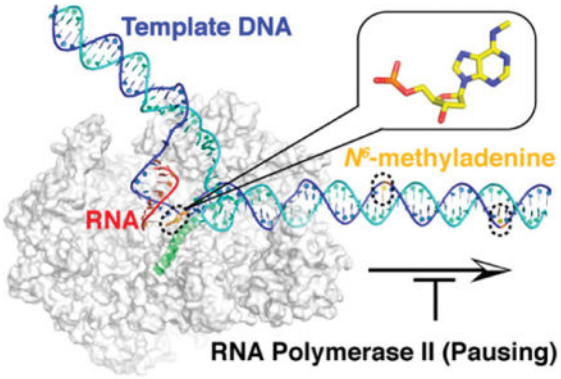

INTRODUCTION

Epigenetic DNA methylation plays important roles in various biological processes.[1] It is well-established that epigenetic mark 5-methylcytosine (5mC) plays crucial roles in regulating gene expression and affects X chromosome inactivation, cellular differentiation, and tumor development.[2–4] Another naturally occurring DNA modification, N^6-methyladenine (N^6-mA or 6mA) (Figure 1a), was previously thought to be absent in metazoans and only present in prokaryotes and a limited number of unicellular eukaryotes.[5,6] Recently, several new reports described the genomic distributions of N^6-mA in many phylogenetically distinct eukaryotes including fungi,[7] green algae,[8] insects,[9] nematodes,[10] frogs,[11] fish,[12] and mammals.[11–13] Interestingly, the genomic abundance of N^6-mA varies from ~0.0001–0.0003% of adenines in plants and mammals to as high as 2.8% of adenines in early diverging fungi.[14] Mounting evidence from different laboratories suggested intriguing functional relevance between N^6-mA and gene expression *in vivo*, despite the underlying mechanism still not being fully understood. The genomic distribution and effects of N^6-mA on gene expression have been found to differ among different eukaryotes. In particular, for certain species associated with high abundance of N^6-mA, such as green algae and fungi, N^6-mA is associated with active gene expression.[8] We previously showed that in *Chlamydomonas reinhardtii* N^6-mA is enriched around the transcription start site (TSS) of more than 14 000 genes (approximately 84% of all genes in this organism), most of which are actively transcribed.[8] Furthermore, RNA-Seq analysis suggested that the presence of N^6-mA at TSS is well correlated with high transcriptional activity.[8] Intriguingly, another recent paper revealed that up to 2.8% of all adenines were methylated in early diverging fungi and these N^6-mAs are clustered at or immediately downstream of the transcription start site (TSS) (~500 bp) of active genes.[7] In *Drosophila melanogaster*, N^6-mA is enriched in transposon bodies and is associated with increased transcriptional activity of transposons.[9] In *Caenorhabditis elegans*, N^6-mA levels were also found to be elevated in mutants with elevated levels of histone H3 lysine 4 dimethylation (H3K4me2), which is a mark associated with active transcription.[10] Taken together, these studies from different species strongly indicate the functional relevance between N^6-mA and gene expression *in vivo*; however, the molecular mechanisms of N^6-mA in gene expression regulation remain elusive.[15,16]

RNA polymerase II (pol II) is responsible for pre-mRNA transcription and is sensitive to various DNA modifications. [17–19] During transcription elongation, RNA pol II travels along the DNA template strand and may encounter all kinds of transcriptional obstructions, including covalent DNA lesions and epigenetic DNA modifications.[17–19] These DNA modifications can affect the template recognition by RNA pol II and lead to distinct transcriptional outcomes (transcriptional pausing/stalling, lesion bypass, arrest) and downstream biological processes.[20–24] Previously, we revealed that RNA pol II is able to detect 5-formylcytosine (5fC) and 5-carboxylcytosine (5caC) via a conserved epi-DNA loop, suggesting the functional role of these oxidized 5-methylcytosines (oxi-mCs) in fine-tuning the transcriptional dynamics of RNA pol II.[25,26] It is not clear whether N^6-mA, a different eukaryotic DNA modification, can be recognized by RNA pol II and influences the transcriptional elongation in a similar manner.

In this study, we systematically investigated the molecular mechanism of how N^6-mA affects RNA pol II transcriptional elongation using biochemical and structural approaches. Our studies revealed that the presence of N^6-mA in the DNA template causes site-specific RNA pol II transcriptional pausing. Based on our combined biochemical and structural data, we propose a unified mechanism of how different epigenetic DNA modifications are recognized by pol II during transcription. This study provides new insights into understanding the potential functional roles of N^6-mA in gene expression.

RESULTS AND DISCUSSION

N^6-mA-Induced Site-Specific pol II Transcriptional Pausing

To investigate whether the presence of N^6-mA affects pol II transcription elongation, we performed *in vitro* transcription assays with purified RNA pol II and scaffolds containing multiple site-specifically modified N^6-mA sites in the DNA template strand (Figure 1b). As shown in Figure 1c, we observed specific transcriptional pausing bands induced by N^6-mA, in comparison with the unmodified DNA template. The pol II pausing sites are located right before the N^6-mA sites (for example, 10mer and 13mer, Figure 1c and Figure S1). Consistently, we only observed a single N^6-mA-induced pol II pausing/stalling for the template containing a single N^6-mA in the DNA template strand (10mer position, Figure S2a). Interestingly, pol II is able to bypass these pausing sites with prolonged incubation in the presence of NTPs, leading to the generation of full-length RNA transcripts.

Transcription factor S-II (TFIIS) facilitates pol II bypass of a variety of obstacles, including certain DNA lesions, pausing sequences, and nucleosomes.[27–29] The apparent stimulatory role of TFIIS on pol II bypass is achieved by its capability to facilitate the cleavage of the backtracking RNA transcript, reactivating backtracked RNA pol II. We then tested whether TFIIS can help RNA pol II bypass the N^6-mA site. Intriguingly, in the presence of TFIIS, we observed prolonged pol II stalling right before it reaches N^6-mA sites (e.g., 10mer position), whereas no obvious TFIIS effect was observed at the same position for control A template (10mer position, Figure 1d and S2c). This result suggests that the forward translocation driven by nucleotide addition opposite the N^6-mA site is much slower than backtracking and TFIIS-stimulated transcript cleavage. Consequently, we observed that TFIIS delays pol II transcriptional bypass of N^6-mA site.

N^6-mA Reduces UTP Incorporation and Promotes pol II Backtracking

To further understand the molecular basis of N^6-mA-induced pol II transcriptional pausing and its impact on transcriptional fidelity, we systematically investigated the effect of N^6-mA on three transcriptional fidelity checkpoints: insertion, extension, and proofreading. For the insertion step, we performed single nucleotide incorporation into the single N^6-mA site and observed ~6-fold slow down of UMP incorporation opposite N^6-mA in comparison with unmodified DNA template (Figures 2a and S3). We also tested the effect of N^6-mA on nucleotide selectivity and found that UTP is still the most efficient substrate to be incorporated opposite the N^6-mA template among all four nucleotide triphosphates (NTPs) (Figure S4). Taken together, these results suggest that while the methylation of adenosine substantially reduces the nucleotide incorporation efficiency, there is no notable effect on nucleotide selectivity. For the extension step, we did not observe any notable effects between the N^6-mA template and unmodified template (Figure S2b). For the proofreading step, we compared TFIIS-stimulated transcript cleavage activity in the N^6-mA modified and unmodified A template. We found that the presence of N^6-mA affects both cleavage rates and translocation register. The cleavage rate in the N^6-mA template is ~2–4-fold faster than that for the unmodified template (Figures 2b and S5). Importantly, the presence of N^6-mA significantly alters the cleavage pattern of RNA transcript. For the scaffold containing a 3′-rU:dA pair, we observed that a majority of cleaved transcript is the $n-1$ cleavage product (black arrow in Figure 2b) derived from pol II at a pretranslocation register (47% ± 1%, 10mer) (Figure S5b), whereas only a minor portion of the cleaved transcript is the $n-2$ cleavage product (blue arrow in Figure 2b) presumably derived from a backtracked pol II (14% ± 0.4%, 9mer) (Figure S5c). In sharp contrast, for the scaffold containing a 3′-rU:N^6-mA pair, we observed that the backtracked-pol II-derived $n-2$ cleavage product became dominant (~46% ± 1%, 9mer) (Figure S5c), whereas $n-1$ cleavage product (derived from pol II at pretranslocation register) dropped to ~31% (Figure S5b). These results suggest that an rU:N^6-mA pair is less stable than its unmodified counterpart (an rU:dA pair). For the N^6-mA template, pol II is more prone to backtracking and subsequent cleavage to generate a shorter RNA transcript ($n-2$). After cleavage, pol II can rapidly incorporate one more nucleotide and pause/stall at $n-1$ position because nucleotide insertion opposite the N^6-mA template is relatively slow. Pol II may experience several cycles of addition–backtracking–cleavage before it can eventually bypass the N^6-mA site.

Structural Basis of the Impacts of N^6-mA on pol II Transcription

To reveal the structural basis of how N^6-mA is accommodated at the pol II active site, we first determined the crystal structure of pol II elongation complex containing a site-specific N^6-mA at the $i+1$ position (EC-I, Table S1). We found that the N^6-mA is located at the canonical $i+1$ template site in a similar manner to the unmodified A template (PDB code 2NVZ)[30] (Figure S6), suggesting that the methylation on the N^6 position of adenine does not alter the template positioning. To further understand how N^6-mA affects UTP incorporation, we solved the crystal structure of pol II elongation complex containing a nonhydrolyzable UTP analogue (UMPNPP) paired with N^6-mA (EC-II, Figures 3 and S7, Table S1). We built UMPNPP into the canonical addition site to fit the electron density in the pol II active site (Figure S7a). Interestingly, while UMPNPP maintained a Watson–Crick base pair with N^6-mA, the UMPNPP base ring rotated ~30° in comparison with its unmodified counterpart

UTP:dA pair (PDB code 2NVZ). This observation suggests a weakened UTP:N^6-mA pair in comparison with canonical UTP:dA pair, which is consistent with previously reported NMR studies.[31] In addition, we noticed additional electron density nearby the UMPNPP triphosphate moiety. An alternative conformation of UTP triphosphate moiety, which can best fit the redundant density, was built into the final model, though other potential interpretations may also exist (Figure S7).

Mechanistic Insights into the Interplay between pol II and Epigenetic DNA Modifications

Several novel mechanistic insights can be obtained by comparing the functional interplays between pol II transcription and two important classes of epigenetic DNA marks: N^6-mA and 5mC (and its oxi-mC derivatives). First, all of these DNA modifications are small and are located at the major groove of DNA duplex, and therefore are better tolerated by pol II active site than bulky DNA modifications or minor-groove modifications. The structural analysis revealed that the matched incoming nucleotide can still form a Watson–Crick base pair with modified DNA template to maintain the correct nucleotide selection. Second, while none of these epigenetic DNA modifications permanently block pol II elongation, they have distinct effects on pol II elongation dynamics and pausing. For example, the methyl group of N^6-mA, but not 5mC, can cause pol II pausing. Among the modifications at the same 5-position of cytosine, 5fC and 5caC but not 5mC and 5hmC lead to pol II pausing.[26] Third, we revealed a novel pol II pausing mechanism by N^6-mA, which is different from 5caC/5fC-induced pol II pausing. Previous study revealed that a conserved epi-DNA loop at the Rpb2 subunit of pol II directly recognizes 5caC/5fC by hydrogen-bonding interactions and has an important role in 5caC/5fC-induced pol II pausing.[26] In contrast, N^6-mA can freely translocate into the canonical $i + 1$ template position, escaping the detection by epi-DNA loop.

Three-Step Model for the Processing of Epigenetic DNA Modifications by pol II

Comparing the molecular mechanisms of 5fC/5caC-induced pol II pausing[26] and N^6-mA-induced pol II pausing, we propose the following three-step model for pol II recognition and processing of epigenetic DNA modifications (Figure 4). The first step of recognition is “template positioning”. In this step, the downstream template base ($i + 2$) crosses over the bridge helix and reaches the canonical $i + 1$ template position. The conserved epi-DNA loop can detect specific epigenetic DNA modifications via specific hydrogen-bonding interactions (such as 5fC/5caC). On the other hand, 5mC and N^6-mA can escape epi-DNA loop detection as their hydrophobic methyl group cannot form hydrogen-bonding interactions. The second step of recognition is termed “substrate positioning and active site assembly”. In this step, the correct substrate is positioned into the addition site to form a Watson–Crick base pair with template base, with the trigger loop and other active site pol II residues undergoing conformational changes to reorganize the pol II active site in order to commit effective nucleotide addition. In this step, 5caC/5fC and N^6-mA compromise substrate positioning and full-assembly of pol II active site through distinct mechanisms. The 5caC:GTP pair has a positional shift from the canonical position of a C:GTP base pair (due to the 5caC–epi-DNA loop interaction) and consequently slows down GMP incorporation. [26] In contrast, the methyl group of the N^6-mA directly weakens the base pairing and consequently slows down UMP incorporation. Notably, the methyl group of 5mC has minimum effect on hydrogen-

bonds within base pair, substrate positioning, and active site assembly in this step; therefore, the GTP incorporation opposite 5mC is as fast as that with unmodified C. The third step of recognition is “post-insertion translocation”. In this step, the newly formed base pair undergoes either forward translocation for the next round of NTP addition or rearward translocation for backtracking. Because backtracking requires the disruption of the 3′-base pair, the hydrogen-bonding strength of the 3′-base pair is crucial. For the N^6-mA template, the weakened base pair between U:N^6-mA promotes backtracking. The presence of N^6-mA increases cleavage rate and changes the cleavage pattern in comparison with unmodified A template (Figure 2b). Interestingly, the presence of 5fC and 5caC also promotes the backtracking population of pol II complex. The TFIIS-mediated cleavage rates for scaffolds containing 5fC and 5caC increased by 5.0- and 2.6-fold, respectively, whereas no noticeable changes were observed in the case of 5hmC and 5mC compared with unmodified C template.[25] Taken together, these results indicate that the presence of 5fC/5caC or N^6-mA greatly shifts pol II from an active population (poised for elongation) to a paused population and promotes pol II stalling and RNA backtracking.

Functional Interplays between N^6-mA and Transcription

Previous studies indicated that N^6-mA can impact transcription indirectly by modifying transcription factor binding or altering chromatin structure. Indeed, the presence of N^6-mA has been shown to modulate transcription factor binding to its target sequence.[32] Furthermore, N^6-mA can also affect pol II transcription by affecting nucleosome positioning, which has a profound effect on every phase of pol II transcription process including initiation and elongation. We previously reported that N^6-mA occurrence at TSS exhibits a periodic pattern with maxima that are complementary to nucleosome binding sites, suggesting that N^6-mA potentially is involved in nucleosome positioning in *C. reinhardtii,*[8] which is also consistent with early observation in *Tetrahymena thermophile*.[33] In this study, we presented that N^6-mA can directly interact with RNA pol II and cause transcriptional pausing/stalling. Considering the distribution patterns of N^6-mA across the genome in different organisms, it is possible that these stalling effects may add a new layer of fine-tuned regulation of Pol II transcription elongation dynamics. The transient Pol II pausing caused by N^6-mA may also provide signals for the recruitment of various transcription elongation factors or chromatin remodeling complexes to induce additional functional consequences. Thus, the mechanisms of N^6-mA in controlling *in vivo* RNA pol II transcription could be multilayer, and future studies are warranted.

CONCLUSION

In summary, here we investigated the effect of N^6-mA on core pol II transcriptional machinery using both biochemical and structural approaches. We found that N^6-mA can cause specific pol II pausing and revealed a novel mechanism of N^6-mA-induced pol II pausing that is different from the previous reported 5caC-induced pol II pausing. We also found that N^6-mA can escape the detection of epi-DNA loop and reach the canonical template position. However, the methyl group of N^6-mA weakens the Watson–Crick base pair with incoming UTP and slows down incorporation opposite N^6-mA. This weakened pairing between UMP:N^6-mA also promotes pol II backtracking. Our results indicate that

pol II can read and distinguish different epigenetic marks, and we propose a three-step recognition mechanism for pol II processing of epigenetic DNA modifications. These findings provide an important new perspective on the functional interplay between epigenetic DNA modification and transcription elongation dynamics.

MATERIALS AND METHODS

Materials

RNA pol II was purified from *Saccharomyces cerevisiae* as previously described.[30,34] The template and nontemplate DNA oligonucleotides were purchased from IDT. The N^6-mA templates and RNA primers were purchased from TriLink Biotechnologies (Figure S8). RNA primers were radiolabeled using [γ-^{32}P]ATP (PerkinElmer) and T4 Polynucleotide Kinase (NEB). The ultrapure NTPs were purchased from Affymetrix.

In Vitro Transcription Assays

The pol II elongation complexes (pol II EC) for the *in vitro* transcription assays were assembled using established methods.[35,36] Briefly, an aliquot of 5′-^{32}P-labeled RNA was annealed with a 1.5-fold amount of template DNA and 2-fold amount of nontemplate DNA to form the RNA/DNA scaffold (final stock concentration 200 nM, defined by RNA concentration) in elongation buffer (20 mM Tris-HCl (pH 7.5), 40 mM KCl, 5 mM $MgCl_2$). An aliquot of the annealed scaffold of RNA/DNA was then incubated with a 4-fold amount of pol II at room temperature for 10 min to ensure the formation of pol II elongation complex. The pol II EC is ready for *in vitro* transcription upon mixing with equal volumes of NTP solution of various concentrations. Final reaction concentrations after mixing were 25 nM scaffold, 100 nM pol II, 5 mM DTT, 5 mM $MgCl_2$, 40 mM KCl, 20 mM Tris-HCl (pH 7.5), and NTP. For transcription assay in the presence of TFIIS, the pol II elongation complex was mixed with equal volume of NTP solution containing 400 nM or 2 μM TFIIS. Final reaction concentrations after mixing were 25 nM scaffold, 100 nM pol II, 5 mM DTT, 5 mM $MgCl_2$, 40 mM KCl, 20 mM Tris-HCl (pH 7.5), and 200 nM or 1 μM TFIIS with NTP in the elongation buffer. The products were quenched by 0.5 M EDTA (pH 8.0) and subsequently analyzed by 16% denaturing urea/TBE PAGE.

Single Turnover Nucleotide Incorporation Assays

The assays were carried out as previously described.[35,36] Briefly, nucleotide incorporation assays were conducted by preincubating 50 nM scaffold with 200 nM pol II for 10 min in elongation buffer to form pol II elongation complex at 22 °C. The preincubated pol II EC was then mixed with an equal volume of solution containing 40 mM KCl, 20 mM Tris-HCl (pH 7.5), 10 mM DTT, 10 mM $MgCl_2$, and 2-fold concentrations of NTP. Final reaction concentrations after mixing were 25 nM scaffold, 100 nM pol II, 5 mM $MgCl_2$, and NTP in elongation buffer. Reactions were quenched at various time points by the addition of one volume of 0.5 M EDTA (pH 8.0) and analyzed as described above. Nonlinear-regression data fitting was performed using Prism 6. The time dependence of product formation was fit to a one-phase association equation to determine the observed rate (k_{obs}).

TFIIS-Stimulated Cleavage Assay

Recombinant TFIIS was purified as described.[25,36] Cleavage reactions were performed by preincubating pol II with various scaffolds as previously described with slight modification. The solution was then mixed with an equal volume of solution containing TFIIS and $MgCl_2$ in elongation buffer. Final reaction conditions were 100 nM pol II, 25 nM scaffold, 200 nM (or 1 μM) TFIIS, and 5 mM $MgCl_2$. Reactions were quenched at various time points by the addition of one volume of 0.5 M EDTA (pH 8.0). Products were separated by denaturing PAGE as described above. The observed cleavage rates (k_{obs}) were determined with two-phase decay fitting equations.

X-ray Crystallography Setup and Analysis

The template DNA, nontemplate DNA, and RNA oligonucleotides were annealed to form the scaffold at a ratio of 1:2:2. The pol II EC was assembled as previously described.[30] The pol II EC crystals were grown using the hanging drop method in solutions containing 390 mM $(NH_4)_2HPO_4/NaH_2PO_4$ (pH 6.0), 50 mM dioxane, 10 mM DTT, and 10–12.5% (w/v) PEG6000. Crystals were transferred in a stepwise manner to cryo buffer as previously described.[30] For the pol II EC with UMP analogue, pol II EC crystals were soaked with 3.5 mM UMPNPP (Jena Bioscience) and 5 mM $MgCl_2$ overnight.

Diffraction data were collected at beamline 8.2.1 at the Advanced Light Source, Lawrence Berkeley National Laboratory, as well as beamline 7.1 at the Stanford Synchrotron Radiation Lightsource. Data were processed with the program MOSFLM[37] and scaled with SCALA from the CCP4 program suite,[38] and then the structure factors were further analyzed by UCLA Diffraction Anisotropy Server.[39] Molecular replacement was done with PHASER of the CCP4 program suite using unmodified pol II EC (PDB code 2NVZ) as a search model. Model building and structural refinement were performed with COOT[40] and PHENIX,[41] respectively. Notably, given the potential rotation flexibility of 6-methyl group and current resolution limitation (3.4 and 3.6 Å resolution), the conformation of the 6-methyl group of N^6-mA cannot be traced from the electron density map unambiguously. We built in the 6-methyl group of N^6-mA based on reported high-resolution structures containing N^6-mA. For the unpaired N^6-mA, the 6-methyl group of N^6-mA was built in a *syn*-conformation, which is energetically preferred.[42–44] For the N^6-mA paired with UMPNPP, the 6-methyl group of N^6-mA was built in an *anti*-conformation (Figure 3c) based on previous high-resolution structures of N^6-mA RNA duplex (PDB code 2MVS)[31] and the complex of *Dpn*I with N^6-mA double-stranded DNA (PDB code 4ESJ and 4KYW).[45] The statistics of data collection and refinement are summarized in Table S1. The quality of these final models was checked with MolProbity.[46] All of the structural figures were rendered in PyMOL (http://www.pymol.org).

Supplementary Material

Refer to Web version on PubMed Central for supplementary material.

Acknowledgments

This work was supported by the National Institutes of Health (Grant R01 GM102362 to D.W. and Grant R01 HG006827 to C.H.). L.H. is a Chicago Fellow, and C.H. is a Howard Hughes Medical Institute Investigator. This research used resources of the Advanced Light Source (8.2.1), which is a DOE Office of Science User Facility under contract no. DE-AC02-05CH11231. Use of the Stanford Synchrotron Radiation Lightsource, SLAC National Accelerator Laboratory, is supported by the U.S. Department of Energy, Office of Science, Office of Basic Energy Sciences under Contract No. DE-AC02-76SF00515. The SSRL Structural Molecular Biology Program is supported by the DOE Office of Biological and Environmental Research and by the National Institutes of Health, National Institute of General Medical Sciences (including P41GM103393). The contents of this publication are solely the responsibility of the authors and do not necessarily represent the official views of NIGMS or NIH. We appreciate beamline staff for their support during our data collection.

References

1. Smith ZD, Meissner A. Nat Rev Genet. 2013; 14:204–220. [PubMed: 23400093]
2. Bestor TH, Edwards JR, Boulard M. Proc Natl Acad Sci U S A. 2015; 112:6796–6799. [PubMed: 25368180]
3. Schubeler D. Nature. 2015; 517:321–326. [PubMed: 25592537]
4. Klose RJ, Bird AP. Trends Biochem Sci. 2006; 31:89–97. [PubMed: 16403636]
5. Ratel D, Ravanat JL, Berger F, Wion D. BioEssays. 2006; 28:309–315. [PubMed: 16479578]
6. Wion D, Casadesus J. Nat Rev Microbiol. 2006; 4:183–192. [PubMed: 16489347]
7. Mondo SJ, Dannebaum RO, Kuo RC, Louie KB, Bewick AJ, LaButti K, Haridas S, Kuo A, Salamov A, Ahrendt SR, Lau R, Bowen BP, Lipzen A, Sullivan W, Andreopoulos BB, Clum A, Lindquist E, Daum C, Northen TR, Kunde-Ramamoorthy G, Schmitz RJ, Gryganskyi A, Culley D, Magnuson J, James TY, O'Malley MA, Stajich JE, Spatafora JW, Visel A, Grigoriev IV. Nat Genet. 2017; 49:964–968. [PubMed: 28481340]
8. Fu Y, Luo GZ, Chen K, Deng X, Yu M, Han D, Hao Z, Liu J, Lu X, Dore LC, Weng X, Ji Q, Mets L, He C. Cell. 2015; 161:879–892. [PubMed: 25936837]
9. Zhang G, Huang H, Liu D, Cheng Y, Liu X, Zhang W, Yin R, Zhang D, Zhang P, Liu J, Li C, Liu B, Luo Y, Zhu Y, Zhang N, He S, He C, Wang H, Chen D. Cell. 2015; 161:893–906. [PubMed: 25936838]
10. Greer EL, Blanco MA, Gu L, Sendinc E, Liu J, Aristizabal-Corrales D, Hsu CH, Aravind L, He C, Shi Y. Cell. 2015; 161:868–878. [PubMed: 25936839]
11. Koziol MJ, Bradshaw CR, Allen GE, Costa AS, Frezza C, Gurdon JB. Nat Struct Mol Biol. 2016; 23:24–30. [PubMed: 26689968]
12. Wu TP, Wang T, Seetin MG, Lai Y, Zhu S, Lin K, Liu Y, Byrum SD, Mackintosh SG, Zhong M, Tackett A, Wang G, Hon LS, Fang G, Swenberg JA, Xiao AZ. Nature. 2016; 532:329–333. [PubMed: 27027282]
13. Ma L, Zhao B, Chen K, Thomas A, Tuteja JH, He X, He C, White KP. Genome Res. 2017; 27:385–392. [PubMed: 28052920]
14. Summerer D. Angew Chem, Int Ed. 2015; 54:10714–10716.
15. Luo GZ, Blanco MA, Greer EL, He C, Shi Y. Nat Rev Mol Cell Biol. 2015; 16:705–710. [PubMed: 26507168]
16. Luo GZ, He C. Nat Struct Mol Biol. 2017; 24:503–506. [PubMed: 28586322]
17. Shin JH, Xu L, Wang D. Transcription. 2016; 7:57–62. [PubMed: 27105138]
18. Shin JH, Xu L, Wang D. Cell Biosci. 2017; 7:9. [PubMed: 28239446]
19. Xu L, Wang W, Chong J, Shin JH, Xu J, Wang D. Crit Rev Biochem Mol Biol. 2015; 50:503–519. [PubMed: 26392149]
20. Fousteri M, Mullenders LH. Cell Res. 2008; 18:73–84. [PubMed: 18166977]
21. Hanawalt PC, Spivak G. Nat Rev Mol Cell Biol. 2008; 9:958–970. [PubMed: 19023283]
22. van Luenen HG, Farris C, Jan S, Genest PA, Tripathi P, Velds A, Kerkhoven RM, Nieuwland M, Haydock A, Ramasamy G, Vainio S, Heidebrecht T, Perrakis A, Pagie L, van Steensel B, Myler PJ, Borst P. Cell. 2012; 150:909–921. [PubMed: 22939620]

23. Wilson MD, Harreman M, Svejstrup JQ. Biochim Biophys Acta, Gene Regul Mech. 2013; 1829:151–157.
24. Lagerwerf S, Vrouwe MG, Overmeer RM, Fousteri MI, Mullenders LH. DNA Repair. 2011; 10:743–750. [PubMed: 21622031]
25. Kellinger MW, Song CX, Chong J, Lu XY, He C, Wang D. Nat Struct Mol Biol. 2012; 19:831–833. [PubMed: 22820989]
26. Wang L, Zhou Y, Xu L, Xiao R, Lu X, Chen L, Chong J, Li H, He C, Fu XD, Wang D. Nature. 2015; 523:621–625. [PubMed: 26123024]
27. Kireeva ML, Hancock B, Cremona GH, Walter W, Studitsky VM, Kashlev M. Mol Cell. 2005; 18:97–108. [PubMed: 15808512]
28. Charlet-Berguerand N, Feuerhahn S, Kong SE, Ziserman H, Conaway JW, Conaway R, Egly JM. EMBO J. 2006; 25:5481–5491. [PubMed: 17110932]
29. Belotserkovskii BP, Mirkin SM, Hanawalt PC. Chem Rev. 2013; 113:8620–8637. [PubMed: 23972098]
30. Wang D, Bushnell DA, Westover KD, Kaplan CD, Kornberg RD. Cell. 2006; 127:941–954. [PubMed: 17129781]
31. Roost C, Lynch SR, Batista PJ, Qu K, Chang HY, Kool ET. J Am Chem Soc. 2015; 137:2107–2115. [PubMed: 25611135]
32. Sugimoto K, Takeda S, Hirochika H. Plant J. 2003; 36:550–564. [PubMed: 14617085]
33. Karrer KM, VanNuland TA. Nucleic Acids Res. 2002; 30:1364–1370. [PubMed: 11884634]
34. Wang D, Bushnell DA, Huang X, Westover KD, Levitt M, Kornberg RD. Science. 2009; 324:1203–1206. [PubMed: 19478184]
35. Kellinger MW, Ulrich S, Chong J, Kool ET, Wang D. J Am Chem Soc. 2012; 134:8231–8240. [PubMed: 22509745]
36. Xu L, Plouffe SW, Chong J, Wengel J, Wang D. Angew Chem, Int Ed. 2013; 52:12341–12345.
37. Battye TG, Kontogiannis L, Johnson O, Powell HR, Leslie AG. Acta Crystallogr, Sect D: Biol Crystallogr. 2011; 67:271–281. [PubMed: 21460445]
38. Collaborative Computational Project, Number 4. Acta Crystallogr, Sect D: Biol Crystallogr. 1994; 50:760–763. [PubMed: 15299374]
39. Strong M, Sawaya MR, Wang S, Phillips M, Cascio D, Eisenberg D. Proc Natl Acad Sci U S A. 2006; 103:8060–8065. [PubMed: 16690741]
40. Emsley P, Cowtan K. Acta Crystallogr, Sect D: Biol Crystallogr. 2004; 60:2126–2132. [PubMed: 15572765]
41. Adams PD, Grosse-Kunstleve RW, Hung LW, Ioerger TR, McCoy AJ, Moriarty NW, Read RJ, Sacchettini JC, Sauter NK, Terwilliger TC. Acta Crystallogr, Sect D: Biol Crystallogr. 2002; 58:1948–1954. [PubMed: 12393927]
42. Sternglanz H, Bugg CE. Science. 1973; 182:833–834. [PubMed: 4746493]
43. Engel JD, von Hippel PH. Biochemistry. 1974; 13:4143–4158. [PubMed: 4606508]
44. Engel JD, von Hippel PH. J Biol Chem. 1978; 253:927–934. [PubMed: 621212]
45. Siwek W, Czapinska H, Bochtler M, Bujnicki JM, Skowronek K. Nucleic Acids Res. 2012; 40:7563–7572. [PubMed: 22610857]
46. Davis IW, Leaver-Fay A, Chen VB, Block JN, Kapral GJ, Wang X, Murray LW, Arendall WB 3rd, Snoeyink J, Richardson JS, Richardson DC. Nucleic Acids Res. 2007; 35:W375–383. [PubMed: 17452350]

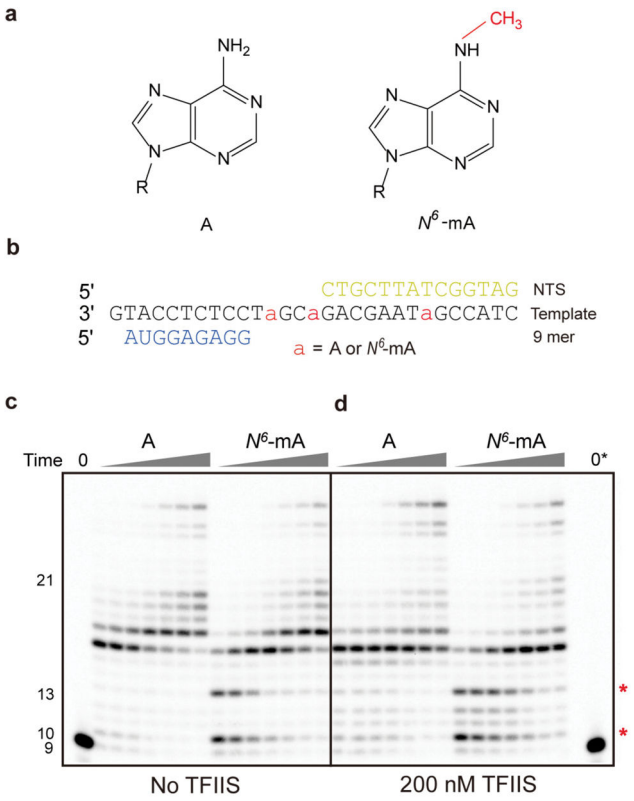

Figure 1.

N^6-Methyladenine (N^6-mA) causes RNA pol II transcriptional pausing. (a) Chemical structure of adenine and N^6-mA. 6-Methyl group is in red. (b) Transcription scaffold containing N^6-mA at DNA template strand. (c, d) N^6-mA cause site-specific pol II pausing (highlighted with *) in the absence of TFIIS (c) and presence of 200 nM TFIIS (d). The concentration of NTPs is 25 μM. Time points are 0, 10 s, 30 s, 1 min, 5 min, 20 min, 1 h, and 3 h, respectively. 0* refers time zero for transcription from N^6-mA template. All experiments were repeated at least 4 times with similar results.

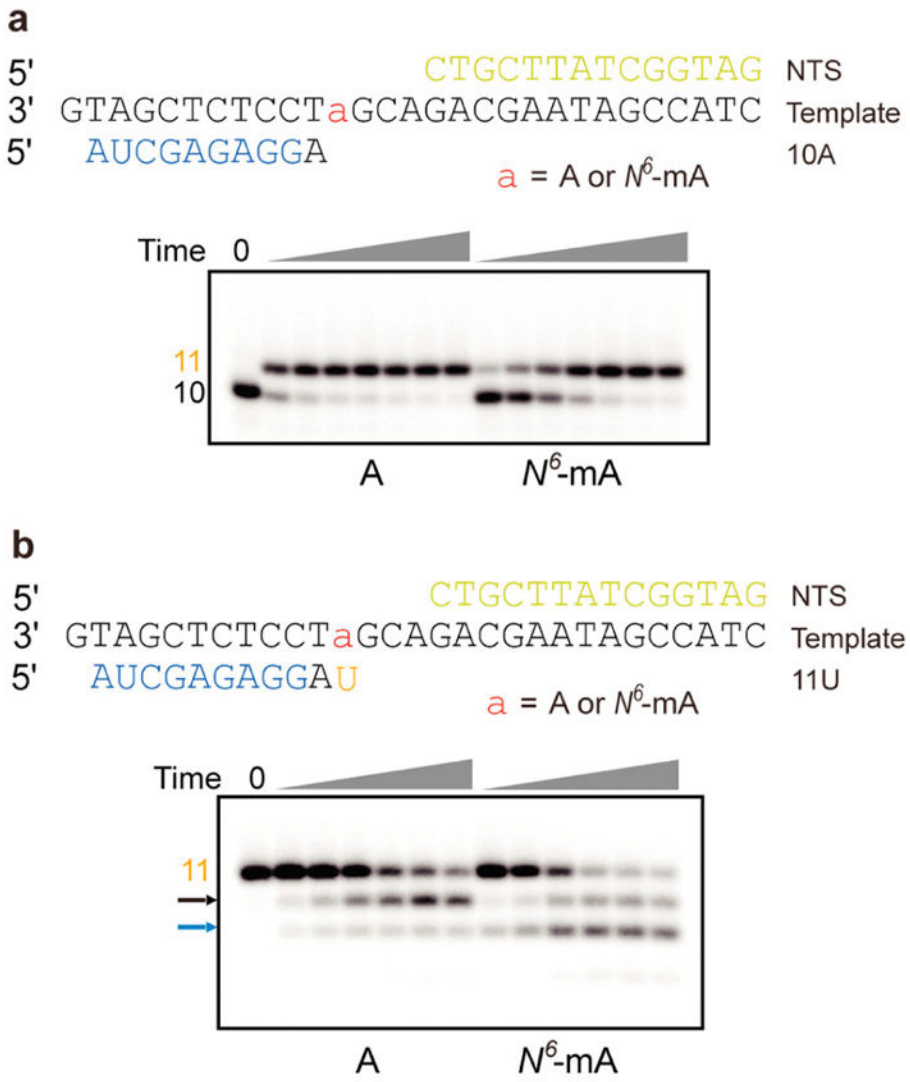

Figure 2.

N^6-mA slows down UMP incorporation and promotes pol II backtracking. (a) The presence of N^6-mA in the DNA template strand leads to slow UMP addition. The concentration of UTP is 25 μM. Time points are 0, 15 s, 30 s, 1 min, 2 min, 5 min, 20 min, and 1 h. (b) The presence of N^6-mA in the DNA template promotes further backtracking revealed by TFIIS-stimulated transcript cleavage assay. Time points are 0, 15s, 1 min, 5 min, 20 min, 1 h, and 3 h, respectively. The DNA/RNA scaffolds are listed with $i + 1$ position highlighted. The $n - 1$ and $n - 2$ cleavage products are highlighted by black and blue arrows, respectively.

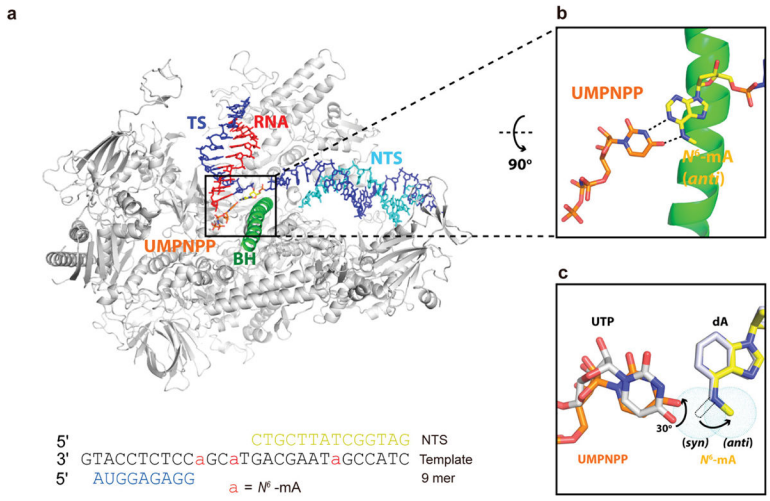

Figure 3.

Crystal structure of N^6-mA-containing RNA pol II elongation complex with UMPNPP soaked (EC-II). (a) Overall structure of pol II EC-II containing an N^6-mA template and UMPNPP. Pol II is shown from the side view as a ribbon model in silver, with the bridge helix (BH) highlighted in green and Rpb2 omitted for clarity. The nucleic acids are shown as stick models: template DNA (TS, blue), nontemplate DNA (NTS, cyan), and RNA (red). The N^6-mA at i + 1 site and one conformation of UMPNPP are highlighted as yellow and orange, respectively. (b) Detailed interaction of UMPNPP:N^6-mA from top view. There exist two conformations of UMPNPP due to the flexibility of triphosphate moiety (more details in Figure S7), but their base groups adopt similar orientation, so the other conformation is omitted for clarity here. Hydrogen bonds are indicated as black dotted lines. (c) UTP and corresponding unmodified dA template from canonical pol II EC (PDB code 2NVZ) are superimposed, which are shown as silver sticks and labeled as black. The potential rotational range of the methyl group of N^6-mA is represented as tiny cyan dots, in which the *syn*-form is shown as dashed stick.

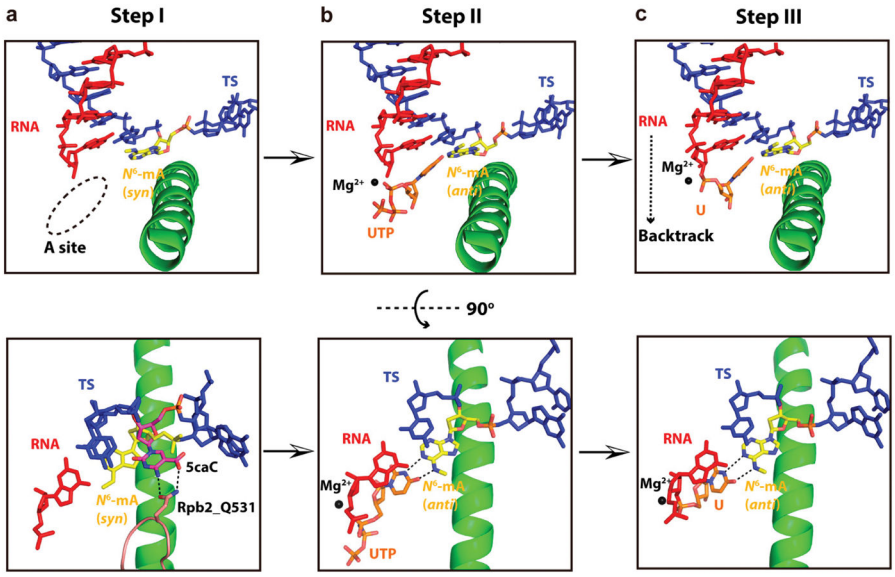

Figure 4.

Model of epigenetic mark N^6-mA recognition and processing by RNA pol II. The upper panel shows the side view, and the lower panel shows the top view. (a) The residue Q531 of Rpb2 (colored as salmon) can capture 5caC (colored as magenta) (PDB code 4Y52) but not N^6-mA of template during template translocation. Addition site (A site) is shown as dotted oval. (b) UTP entry is slowed down due to impaired stability of UTP:N^6-mA pair. (c) After UMP addition, the extended RNA is prone to backtracking due to the impaired stability of UMP/N^6-mA pair.